A Letters Journal Exploring the Frontiers of Physics

August 2014

EPL, **107** (2014) 34007
doi: 10.1209/0295-5075/107/34007

www.epljournal.org

Tuning the dispersion relation of a plasmonic waveguide via graphene contact

Yu Zhou, Cheng Wang, Di-Hu Xu, Ren-Hao Fan, Kun Zhang, Ru-Wen Peng[a], Qing Hu and Mu Wang

National Laboratory of Solid State Microstructures and Department of Physics, National Center of Microstructures and Quantum Manipulation, Nanjing University - Nanjing 210093, China

received on 19 June 2014; accepted by M. Polini on 11 July 2014
published online 30 July 2014

PACS 42.79.Gn – Optical waveguides and couplers
PACS 78.67.Wj – Optical properties of graphene
PACS 42.65.Hw – Phase conjugation; photorefractive and Kerr effects

Abstract – In this work, we have investigated experimentally and theoretically the dispersion relation of a plasmonic slab waveguide, where the thin gold film with nano-aperature arrays is sandwiched by graphene and a silica layer on a silicon chip. It is shown that the plasmonic slab waveguides are compatible with silicon technology. We have found that when the light waves irradiate the nanostructured waveguides with or without graphene, surface plasmon polaritons are always excited at the metal-dielectric interface due to the interaction between the surface charge oscillation and the electromagnetic field of the light. But in the slab waveguide with graphene, the resonant dips definitely shift in the reflection spectra, which indicates that the contact of graphene can tune the dispersion relation of the waveguide in the visible regime. Experimental measurements on optical reflections are in good agreement with calculated plasmonic band structures. Further calculations show that the dispersion relation of plasmonic slab waveguides can be tuned by electron doping and the nonlinear effect of graphene. The investigations provide a way to actively control the dispersion relation of plasmonic waveguides on silicon chips and benefit the development graphene-related active optical devices.

Introduction. – Surface plasmon polariton (SPP) is the surface wave that forms at the metal-dielectric interface [1]. It can propagate along the interface for a rather long distance and can confine light into deep subwavelength volumes beyond the diffraction limit [1,2]. Nowadays the SPP waveguide made by a noble-metal slab is regarded as a fundamental component in the plasmonic circuits [3,4]. Several approaches have been introduced to excite the SPPs via overcoming the momentum mismatch between the light in free space and the surface wave, including prism coupling [5,6], defect scattering [7], and periodic patterning [8]. Periodic patterning uses a reciprocal vector to satisfy the momentum match and has been successfully used to launch SPPs at a specific wavelength or frequency [9,10]. The excited wavelength is very sensitive to the surface condition which reminds us that one can alter the dispersion relation of the plasmonic waveguides by modifying their surface. Recently, there has been an increasing interest in graphene application in plasmonics [11,12]. Graphene-noble metal contact can serve as a good foundation for enhanced light-matter interaction [13–15], molecule sensing [16–19] and low loss plasmonic applications [20,21] due to the interaction between graphene electron and the surface plasmon. The properties of graphene can be tuned by doping or the nonlinear effect [22–25], providing a new way for a tunable graphene-related device. In this work, we design a plasmonic slab waveguide that is compatible with silicon technology, and tune the dispersion relation of the waveguide via graphene contact. Shifts of the resonances in the reflection spectra are obvious and experimental measurements are in good agreement with calculated plasmonic band structures.

Experiment results and theoretical model. –

Sample fabrication and measurement. Since silicon is very lossy in the visible range, an isolating layer is necessary to design a plasmonic waveguide compatible with silicon technology. Figure 1 is a schematic view of our

[a] Present address: National Laboratory of Solid State Microstructures and Department of Physics, Nanjing University - Nanjing 210093, China; E-mail: rwpeng@nju.edu.cn (corresponding author)

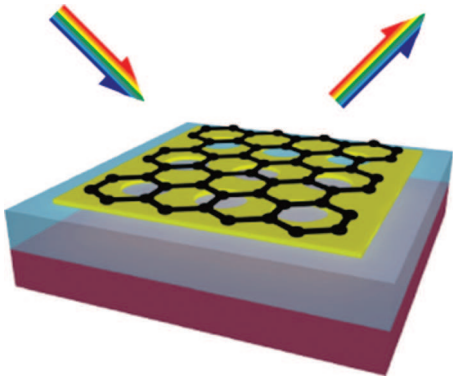

Fig. 1: (Colour on-line) Design of the slab plasmonic waveguide. Materials from bottom to top are, respectively, silicon chip, a 300 nm SiO2 layer, a 40 nm gold film and graphene.

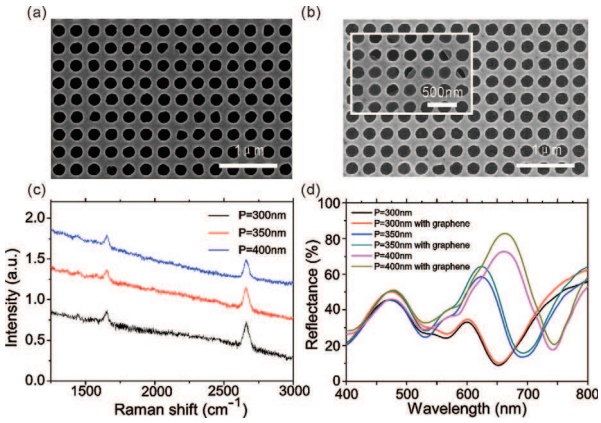

Fig. 2: (Colour on-line) (a) SEM image of the sample with period of 300 nm before the deposition of graphene. (b) SEM image of the sample with period of 300 nm after the deposition of graphene. Inset: region where the graphene cracks. (c) Raman spectra of three samples with period of 300 nm, 350 nm and 400 nm. (d) Reflection spectra of the three samples before and after the deposition of graphene.

design. In the experiment, a 300 nm SiO2 layer is formed on top of the Si substrate by thermal oxidation, which is thick enough to isolate the Si substrate from the metal waveguide above. The plasmonic waveguide is made of a 40 nm Au film fabricated by magnetron sputtering. To effectively excite the SPPs, periodic holes are milled in the metal film using a focus ion beam (FIB). The radius of the hole is designed to be 100 nm to ensure strong interaction with light in the visible range, and three samples with period of 300 nm, 350 nm and 400 nm are fabricated. A graphene layer was firstly grown by the chemical vapor deposition (CVD) method on copper and then transferred onto the waveguide by the PMMA method [26]. Figure 2(a) and fig. 2(b) show the SEM images of samples with and without graphene, respectively. The inset in fig. 2(b) indicates the region where the graphene is cracked. Figure 2(c) shows the Raman spectra of three samples after the deposition of graphene where the broad baseline is the photoluminescence of Au. Two sharp peaks on the baseline are the G and 2D modes of graphene. The dominant 2D peaks indicate that the graphene is indeed a monolayer [27,28]. The reflection spectra, in fig. 2(d), are measured before and after the deposition of graphene using a micro-spectrophotometer (Craic). We can see that after the deposition of graphene, resonant dips redshift.

Theoretical model. We use the commercial finite difference time domain (FDTD) software package (Lumerical FDTD Solutions) to calculate the band structure of the waveguide. In the calculation, the graphene layer is modeled as an ultra-thin metallic layer whose optical conductivity is exactly the optical conductivity of the pristine graphene ($\pi e^2/2h$) in a visible range. We take the theoretical value of the graphene thickness of 0.35 nm in the calculation. All the geometry parameters are set as the same as those in the experiment. Figure 3 shows the band structures of the waveguides plotted in ω-k diagrams, which are calculated from the reflection dips under different incident angles. The right/left side of the ω-k diagrams describes band structure before/after the deposition of graphene. Figures 3(a)–(c) are band structures under TE incident. We can see that for all three samples two modes exist which behave differently as the period increases. The mode which redshifts with the period is the SPP mode and the other one is the cavity mode. Figures 3(d)–(f) are the band structures under TM incident. Except for the cavity modes, there also exist SPP modes which can be more efficiently excited by TM rather than by TE illumination. The dispersion relations of the SPP mode clearly show the plasmonic characters and redshift while increasing the period of the aperture arrays. At the centre of the band structure where $k_{//} = 0$, the resonance dips stagger from each other. This is the case under normal incident corresponding to the reflection spectra in fig. 2(d). To further analyze the modes, we investigate the field distribution at the resonances. Figure 4 shows the field distributions from the cross-sectional and top view of the structure whose period is 400 nm. Figure 4(a) and fig. 4(b) describe the field profile at 523 nm from which we can conclude that this is the cavity mode. The hole and the structures beneath form a cavity and the cavity mode can be excited under both TE and TM illuminations. Figure 4(c) and fig. 4(d) show the field profile at 731 nm. The propagation of the SPP along the metal layer can be clearly seen, which indicates that such mode is the SPP mode. Therefore, there are two kinds of modes in the structure, one is the cavity mode and the other is the SPP mode. We draw this conclusion based on the field profiles and the reflection spectra at the resonances. For the cavity mode, the field intensity is rather weak at the metal-dielectric interface and the resonance is in the silica layer, as shown in fig. 4(a); while there is no sign of wave propagation at the metal surface, as shown in fig. 4(b). Another proof of the cavity mode is that it does not scale with the period, as described in fig. 3(a)–(f). Unlike the cavity mode, the SPP mode profile has maximum field intensity at the

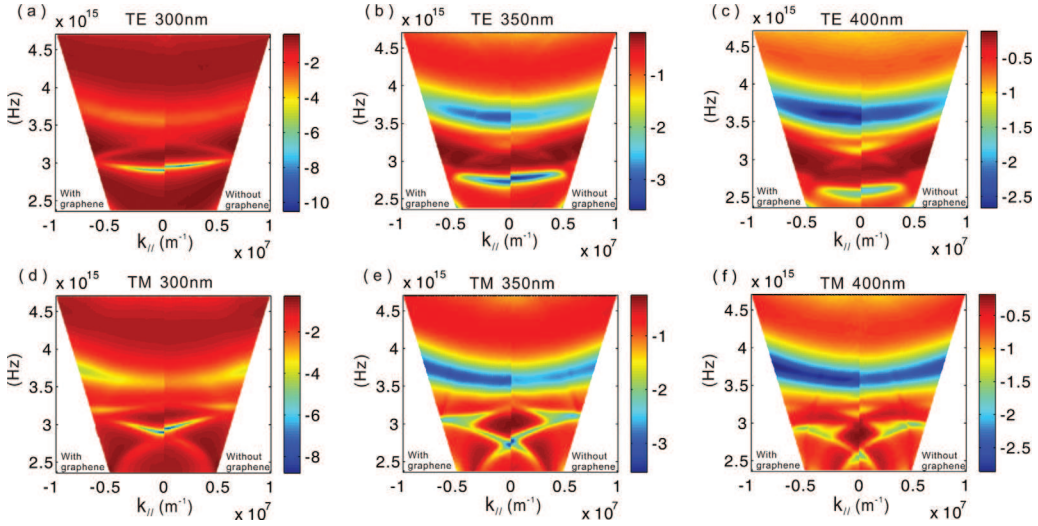

Fig. 3: (Colour on-line) Panels (a), (b), (c) are, respectively, the band structure of the sample with period of 300 nm, 350 nm and 400 nm under TE illuminations. Panels (d), (e), (f) are, respectively, the band structure of the sample with period of 300 nm, 350 nm and 400 nm under TM illuminations.

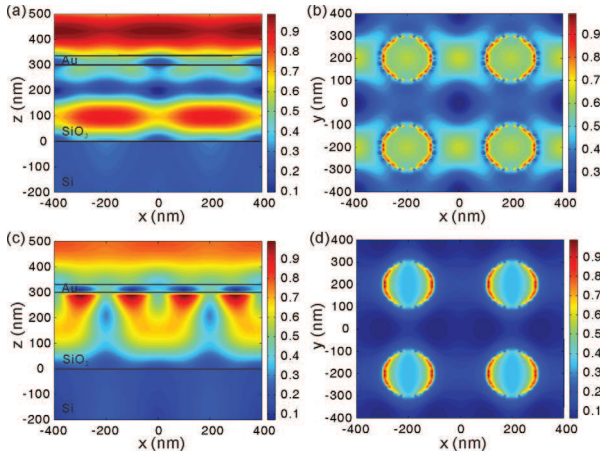

Fig. 4: (Colour on-line) (a) Cross-sectional and (b) top views of the cavity mode at 523 nm. (c) Cross-sectional and (d) top views of the SPP mode at 731 nm.

metal-dielectric interface (in fig. 4(c)) and the wave propagating along the metal film is rather obvious (in fig. 4(d)). Furthermore, the resonance wavelength scaling with the period, described in fig. 3(d)–(f), also indicates the existence of the SPP mode.

Next, we compare the simulation results under normal incident with the measured ones, just as plotted in fig. 5. For all samples with different periods, the simulated results agree with the measured ones very well. Two kinds of modes are all clearly identified in the reflection dips. In the experiment, the reflection dips for the SPP mode are shallower and broader than the calculated ones. This can be attributed to the disorder effect in sample fabrications. The disorder of the hole period and radius will scatter and partially block the propagating SPPs, thus it will decrease the resonance depth and broaden the dip. We further plot the discrepancy between simulation and experiment for the cavity mode and the SPP mode (defined as Δ) as a function of the resonant wavelength in fig. 5(g). Just as we can see, there exist only small deviations between the theoretical and the experimental results.

Tuning the dispersion relation. – One of the great advantages of the graphene over other materials is that its properties can be easily tuned either by the electron doping or the nonlinear effect. Here we theoretically investigate that the dispersion relation of the waveguide can be tuned via graphene contact.

Electron doping effect. The interaction between light and graphene can be described by the optical conductivity which can be calculated by summing the interband and intraband conductivities. More explicitly [29,30],

$$\sigma_{\rm inter}(\omega) = i\frac{e^2\omega}{\pi}\int_{\Delta}^{\infty} {\rm d}\varepsilon \frac{1+\Delta^2/\varepsilon^2}{(2\varepsilon)^2-(\hbar\omega+i\Gamma)^2} \times \Big[f(\varepsilon-E_F)-f(-\varepsilon-E_F)\Big], \quad (1)$$

$$\sigma_{\rm intra} = i\frac{e^2/\pi\hbar^2}{\omega+i/\tau}\int_{\Delta}^{\infty} {\rm d}\varepsilon(1+\Delta^2/\varepsilon^2) \times \Big[f(\varepsilon-E_F)+f(\varepsilon+E_F)\Big], \quad (2)$$

where $f(\varepsilon-E_F)$ is the Fermi distribution function with the Fermi energy E_F, Γ describes the broadening of the interband transitions, and τ is the momentum relaxation time due to intraband carrier scattering. The bandgap 2Δ, due to any interaction that breaks the symmetry between A and B atoms in the unit cell of graphene, is set to be zero

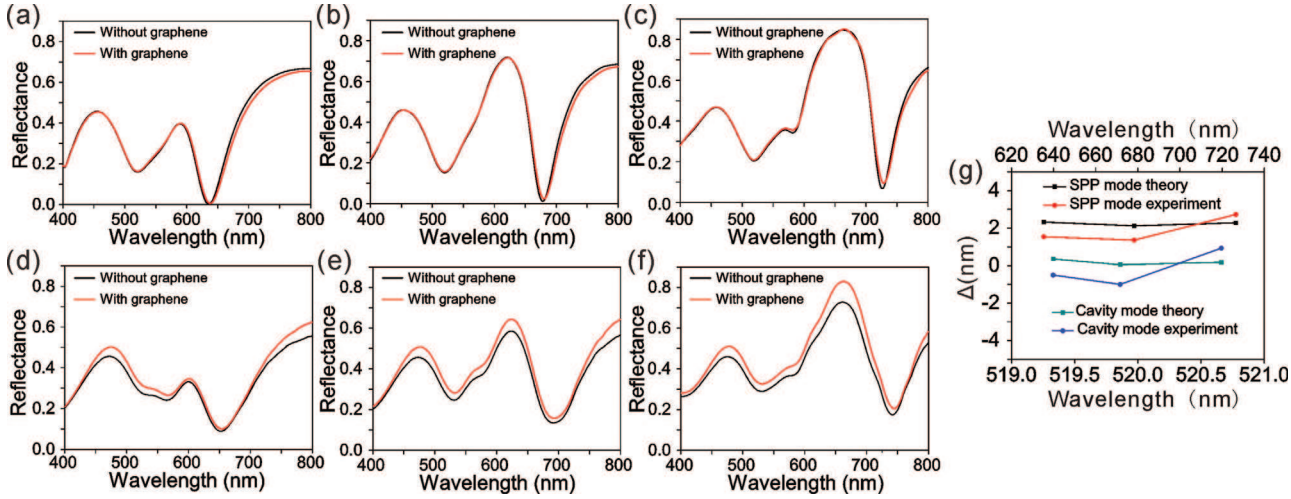

Fig. 5: (Colour on-line) Calculated reflection spectra of the sample with period of (a) 300 nm, (b) 350 nm and (c) 400 nm, respectively. Measured reflection spectra of the sample with period of (d) 300 nm, (e) 350 nm and (f) 400 nm, respectively. (g) Resonances shift of the cavity mode and the SPP mode as a function of the resonant wavelength.

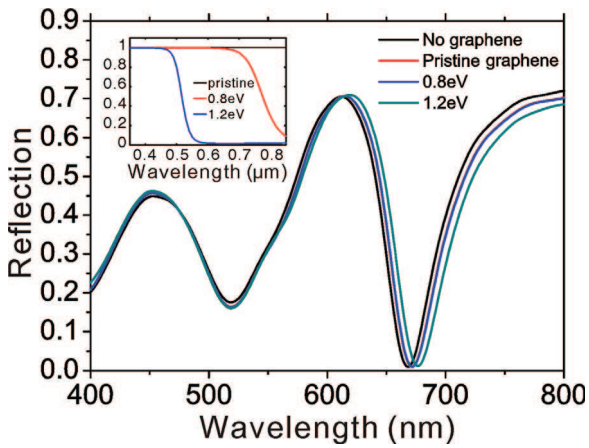

Fig. 6: (Colour on-line) Reflection spectra for different doping levels of graphene. The Fermi level is set at 0 eV, 0.8 eV or 1.2 eV. Inset: real part of the graphene conductivity, in the unit of $\pi e^2/2h$.

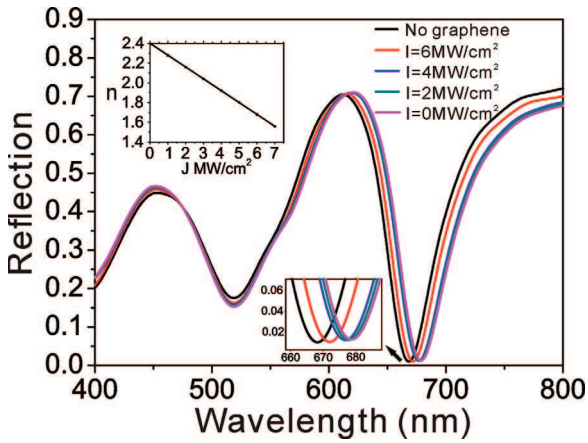

Fig. 7: (Colour on-line) Reflection spectra under different pump intensities. Upper inset: the refractive index of graphene as a function of the pump intensity. Lower inset: enlarged figure near the SPP modes.

in this paper. Switching on and off the interband transition by tuning the Fermi level provides the way to tune the optical conductivity thus the optical response of the graphene. Figure 6 shows the reflection spectra for different doping levels of graphene and the inset plots the corresponding total optical conductivities. Just as we can see, the conductivity decreases drastically when switching off the interband transition, so the corresponding reflection dip shifts. Thus, the dispersion relation of such waveguide can be tuned by doping the graphene, for example, via backgate voltage.

Nonlinear effect. It has been discovered that graphene has a giant nonlinear refractive index $n_2 = -1.2 \times 10^{-7}\,\mathrm{cm}^2/\mathrm{W}$ [24] and an ultrafast response of the order of 1 ps due to fast carrier relaxation dynamics. Therefore, graphene is an excellent nonlinear optical material with an ultrafast response and high third-order optical nonlinearity. In this way, we can tune the dispersion relation of our waveguide by introducing an intense optical pump. In the simulation, we set the effective linear refractive index n_0 of graphene to be 2.4 as previously used by Zhu *et al.* [25]. The effective refractive index n of graphene changes as a function of the pump intensity I as $n = n_0 + n_2 I$, where n_0 and n_2 are the effective linear and nonlinear refractive indexes of graphene, respectively. The upper inset of fig. 7 shows the refractive index of graphene as a function of the pump intensity, which decreases linearly as the pump intensity increases due to the negative nonlinear refractive index. Thus, the resonance dips blueshift as the pump intensity increases, as shown in the lower inset of fig. 7. Therefore, the dispersion relation of the plasmonic waveguide can be tuned based on the nonlinear effect of graphene.

Conclusions. – In this paper, a plasmonic waveguide compatible with silicon technology has been studied and the dispersion relation of the waveguide has been tuned via graphene contact. We have proposed a model of graphene in the visible range for FDTD calculation and the results coincide with the experiment. Two kinds of resonance, *i.e.* the cavity mode and the SPP mode, have been clearly identified and the effect of graphene has been discussed. Furthermore, by doping the graphene or using the nonlinear effect, we can theoretically tune the dispersion relation of the waveguide. Our work presents a useful effort in exploring hybrid Si/graphene plasmonic waveguides and provides potential applications for tunable opto-devices.

* * *

This work was supported by the MOST of China (Grants No. 2012CB921502 and 2010CB630705) and the NSFC (Grants No. 11034005, 11321063, and 91321312).

This article has been submitted by participants at the META'14 event in Singapore in May 2014. EPL supports the META series by providing annual sponsorship. The scientific content has been peer reviewed under the same guidelines and criteria as all other EPL letters.

REFERENCES

[1] Barnes W. L., Dereux A. and Ebbesen T. W., *Nature*, **424** (2003) 824.
[2] Gramotnev D. K. and Bozhevolnyi S. I., *Nat. Photon.*, **4** (2010) 83.
[3] Ebbesen T. W., Genet C. and Bozhevolnyi S. I., *Phys. Today*, **61**, issue No. 5 (2008) 44.
[4] Sorger V. J., Oulton R. F., Ma Ren-Min and Zhang X., *MSR Bull.*, **37** (2012) 728.
[5] Kretschmann E. and Raether H., *Z. Naturforsch. A*, **23** (1968) 2135.
[6] Otto A., *Z. Phys.*, **216** (1968) 398.
[7] Hecht B., Bielefeldt H., Novotny L., Inouye Y. and Pohl D. W., *Phys. Rev. Lett.*, **77** (1996) 1889.
[8] Ritchie R. H., Arakawa E. T., Cowan J. J. and Hamm R. N., *Phys. Rev. Lett.*, **21** (1968) 1530.
[9] Tang Z. H., Peng R. W., Wang Z., Wu X., Bao Y. J., Wang Q. J., Zhang Z. J., Sun W. H. and Wang Mu, *Phys. Rev. B*, **76** (2007) 195405.
[10] Gao Feng, Li De, Peng Ru-Wen, Hu Qing, Wei Kuang, Wang Q. J., Zhu Y. Y. and Wang Mu, *Appl. Phys. Lett.*, **95** (2009) 011104.
[11] Grigorenko A. N., Polini M. and Novoselov K. S., *Nat. Photon.*, **6** (2012) 749.
[12] Bao Q. L. and Loh K. P., *ACS Nano*, **6** (2012) 3677.
[13] Koppens F. H. L., Chang D. E. and García de Abajo F. J., *Nano Lett.*, **11** (2011) 3370.
[14] Hao Q. Z., Wang B., Bossard J. A., Kiraly B., Zeng Y., Chiang I-Kao, Douglas L. J., Werner H. and Huang T. J., *J. Phys. Chem. C*, **116** (2012) 7249.
[15] Zhu X. L., Shi L., Schmidt M. S., Boisen A., Hansen O., Zi J., Xiao Sanshui and Mortensen N. A., *Nano Lett.*, **13** (2013) 4690.
[16] Salihoglu O., Balci S. and Kocabas C., *Appl. Phys. Lett.*, **100** (2012) 213110.
[17] Liu Y., Dong X. and Chen P., *Chem. Soc. Rev.*, **41** (2012) 2283.
[18] Kravets V. G., Schedin F., Jalil R., Britnell L., Gorbachev R. V., Ansell D., Thackray B., Novoselov K. S., Geim A. K., Kabashin A. V. and Grigorenko A. N., *Nat. Mater.*, **12** (2013) 304.
[19] Reckinger N., Vlad A., Melinte S., Colomer Jean-François and Sarrazin M., *Appl. Phys. Lett.*, **102** (2013) 211108.
[20] Rast L., Sullivan T. J. and Tewary V. K., *Phys. Rev. B*, **87** (2013) 045428.
[21] Varykhalov A., Scholz M. R., Kim Timur K. and Rader O., *Phys. Rev. B*, **82** (2010) 121101.
[22] Wu R., Zhang Y., Yan S., Bian F., Wang W., Bai X., Lu X., Zhao J. and Wang E., *Nano Lett.*, **11** (2011) 5159.
[23] Nikolaenko A. E., Papasimakis N., Atmatzakis E., Luo Zhiqiang, Shen Z. X., De Angelis F., Boden S. A., Di Fabrizio E. and Zheludev N. I., *Appl. Phys. Lett.*, **100** (2012) 181109.
[24] Zhang H., Virally S., Bao Q., Ping L. K., Massar S., Godbout N. and Kockaert P., *Opt. Lett.*, **37** (2012) 1856.
[25] Zhu Y., Hu X., Yang H. and Gong Q., *Sci. Rep.*, **4** (2014) 3752.
[26] Li X., Zhu Y., Cai W., Borysiak M., Han B., Chen D., Piner R. D., Colombo L. and Ruoff R. S., *Nano Lett.*, **84** (2009) 4359.
[27] Ferrari A. C., Meyer J. C., Scardaci V., Casiraghi C., Lazzeri M., Mauri F., Piscanec S., Jiang D., Novoselov K. S., Roth S. and Geim A. K., *Phys. Rev. Lett.*, **97** (2006) 187401.
[28] Ferrari A. C. and Basko D. M., *Nat. Nanotechnol.*, **8** (2013) 235.
[29] Mak K. F., Sfeir M. Y., Wu Yang, Lui C. H., Misewich J. A. and Heinz Tony F., *Phys. Rev. Lett.*, **101** (2008) 196405.
[30] Dawlaty J. M., Shivaraman S., Strait J., George P., Chandrashekhar M., Rana F., Spencer M. G., Veksler D. and Chen Y., *Appl. Phys. Lett.*, **93** (2008) 131905.